RSC Advances

This is an *Accepted Manuscript*, which has been through the Royal Society of Chemistry peer review process and has been accepted for publication.

Accepted Manuscripts are published online shortly after acceptance, before technical editing, formatting and proof reading. Using this free service, authors can make their results available to the community, in citable form, before we publish the edited article. This *Accepted Manuscript* will be replaced by the edited, formatted and paginated article as soon as this is available.

You can find more information about *Accepted Manuscripts* in the Information for Authors.

Please note that technical editing may introduce minor changes to the text and/or graphics, which may alter content. The journal's standard Terms & Conditions and the Ethical guidelines still apply. In no event shall the Royal Society of Chemistry be held responsible for any errors or omissions in this *Accepted Manuscript* or any consequences arising from the use of any information it contains.

ROYAL SOCIETY OF CHEMISTRY

www.rsc.org/advances

RSC Advances Accepted Manuscript

pH-dependent size and structural transition in P123-micelles induced gold nanoparticles

P. Chatterjee and S. Hazra*

The influence of the pH-value of the aqueous solution of P123-micelles on the growth and formation of gold nanoparticles (AuNPs), which is of immense importance for their controlled growth in a simple single-step synthesis process, was investigated using time-evolution optical absorption spectroscopy, dynamic light scattering and transmission electron microscopy techniques. The size and structures of the AuNPs are found pH-dependent, even within basic region, with transition near pH $\approx$ 9.5, though the free P123-micelles remain almost unchanged. Below this pH-value, the slow reduction rate of gold ions creates less number of nucleation centers, which through autocatalytic thermodynamically controlled reduction (ATCR), initially formed chain-like aggregated small AuNPs (of different chain length) and subsequently through further diffusion and coalescence, formed well-faceted near symmetrical large AuNPs of size $\gg$ 19 nm, the size of the free P123-micelles. Above this pH-value, the fast reduction rate of the gold ions creates large number of nucleation centers. The growth of which is well restricted by the limited amount of available gold ions for the ATCR and also due to the metal-polymer hydrophobic and polymer-water hydrophilic interactions. Accordingly, controlled growth of the majority of the centers takes place through ATCR, diffusion and early capping through near individual micelles to form isolated symmetric small AuNPs of size $<$ 19 nm, with narrow size distribution, which are really intended for the different applications and fundamental studies. However, minority (but not insignificant amount) of the centers still remain in very small sizes and trapped inside the large micellar assemblies or even in the near atomic states, which create hindrance in the yield of the isolated small AuNPs.

1 Introduction

Metal nanoobjects are attracting significant attention because of their fascinating size-dependent optical, magnetic, electronic, and catalytic properties. Among them, gold nanoparticles (AuNPs) with desirable structures and functions are of special interest due to their various applications in photonics, sensors, catalysis and biomedicine.[1–12] Reduction, nucleation, stabilization and dispersion are the major steps for the synthesis of metal nanoparticles with desirable structures, morphology (size and shape) and functions. Stabilization and dispersion of AuNPs are achieved by covering them with different macromolecules such as polymers, surfactants and proteins through various interactions like covalent bond, hydrogen bond, electrostatic forces, and so forth.[2–5,7–11]

AuNPs are generally synthesized using solution-phase method by chemical reduction of precursor gold ions involving organic solvents and then chemically attached with organic molecules that counterbalance the van der Waals attraction occurring between the nanoparticles.[5,11,13] Such AuNPs are difficult to disperse in water, which is sometime hindrance for further surface modification and functionalization as essential for particular applications. Compared to such a synthesis process, another environment-friendly method where AuNPs can be synthesized in aqueous media from the chemical reduction of gold ions by reducing agents such as citric acid and ascorbic acid in the presence of one or more water-soluble polymers or surfactants as capping agents, and with the support of externally supplied energy like, photoirradiation, ultrasound irradiation, or heating is developed.[5,11,14–16] In this process the colloidal stability of the nanoparticles is mainly via the chemical binding of ligands at the surface. Such binding may again alter the intended properties of the nanoparticles.

To maintain the intended properties of the nanomaterials, lots of work are going on to develop simple, versatile and economically viable methods for the preparation of AuNPs in a size- and shape-controlled manner where the ligands (like, surfactants, macromolecules) adsorb physically over the surface of the nanoparticles. In this direction, various attempts are made to synthesize stable AuNPs at ambient temperature in a single step process from aqueous solution of gold salt using water-soluble triblock copolymer (TBP) which acts as both reducing and stabilizing agent due to its amphiphilic nature.[5,12,17–21] TBPs belong to a special category of nonionic surfactants which have two or more different monomer linked by covalent bonds. The most widely used TBPs are poly(ethylene oxide)-poly(propylene oxide)-poly(ethylene oxide) (PEO-PPO-PEO with the commercial name of Pluronics) with different

Saha Institute of Nuclear Physics, 1/AF Bidhannagar, Kolkata 700064, India. E-mail: satyajit.hazra@saha.ac.in

Manuscript updated: July 27, 2015

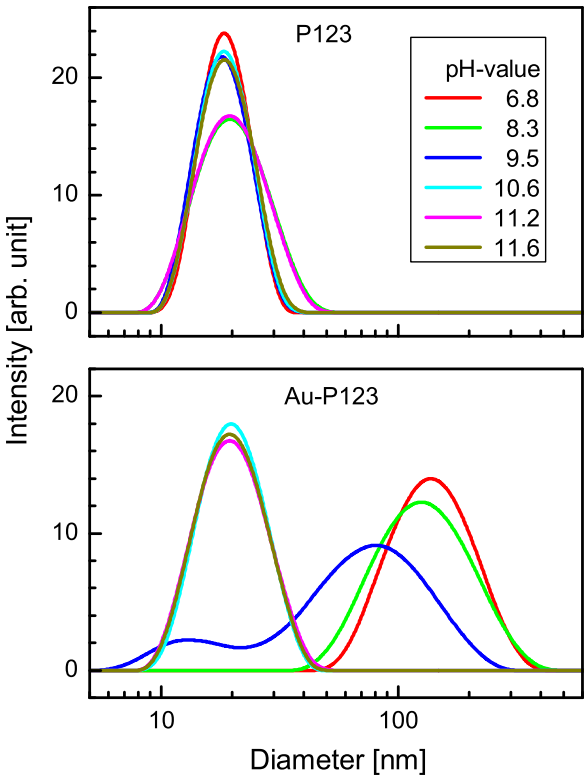

Fig. 1 Size distribution plots, obtained from DLS data, for the mixed binary (P123 + water) and ternary ($HAuCl_4$ + P123 + water) solutions of different pH values (data taken after 3 h of mixing).

numbers of PEO and PPO blocks. In the aqueous solution, TBPs form micelles with hydrophobic PPO as core and hydrophilic PEO as corona.[12,19–24] The corona is in the form of surface cavity which is in direct contact with the aqueous solution and constitute the micelle-solution interface of a TBP micelle. TBPs are mainly used to synthesize AuNPs because of their ability to reduce gold ions following the three steps: i) reduction of gold ions in the surface cavity of TBP micelles in the solution and formation of gold clusters, ii) adsorption of micelles on gold clusters and reduction of gold ions on the surfaces of these gold clusters, and iii) growth of gold particles in steps and finally its stabilization by TBP micelles.[17,18,25] So any change in the micelle environment (namely ratio of PEO and PPO block lengths, molecular weight of TBP, concentration of TBP and/or Au salt in solution, temperature of mixed solution, etc.) is expected to cause a significant change in the reduction, growth, morphology and also stabilization of nanoparticles.

Recently, researchers have paid attention to reveal the influence of different parameters of TBP micelles in the formation and growth mechanism of AuNPs.[19–21,26] One such important parameter is the pH-value of the aqueous TBP micellar solution, which is relatively less studied.[26] It is found that in low pH region the reduction of gold ion is very slow, which resulted in the formation of unstable large aggregated nanoparticles of various shape, whereas with increase of pH value of micellar solution, the reduction process of gold ion is accelerated and highly-stabilized nanoparticles with small average diameter and narrow size distribution are formed,[26] which is in contrary to the other processes where reducing reagents, such as sodium citrate or ascorbic acid are utilized.[2,27] It is clear from different studies that the pH-value strongly influence the reaction kinetics. However, the exact influence of the pH-value of the micellar solution on the growth kinetics of nanoparticles is not very clear, which is essential for the better control in the growth, size, shape, stability and the amount of nanoparticles.

In this paper, we have tried to understand the role of the pH-value of the TBP micellar solution on the simultaneous reduction of gold ion and formation of AuNPs using complementary techniques. For that, the evolution and final state of mixed aqueous solution, containing TBP and gold salt, of different pH-value, were monitored using ultraviolet-visible (UV-vis) spectroscopy[28–37] and dynamic light scattering (DLS)[37–39] techniques, respectively, while the morphology of the AuNPs and aggregates in the final states were imaged through transmission electron microscopy (TEM).[40] Presence of isolated large AuNPs and large micelles loaded with small AuNPs are clearly evident. The size of the isolated AuNPs decreases as the pH of the solution is varies from normal to high, with a transition near pH ≈ 9.5. Below this value the size is much greater than that of the micelles, while above this value the size is less than that of the micelles. Also, a strong shift in the peak at 325 nm, originates from the LMCT band between $AuCl_4^-$ ions and PEO surface cavities, has been observed. Attempted has been made to correlate these interesting observations.

2 Experimental details

2.1 Materials

Pluronic TBP of P123 [$HO(CH_2CH_2O)_{20}$ $(CH_2CH(CH_3)O)_{70}$ $(CH_2CH_2O)_{20}H$, M_w=5800] and gold salt of hydrogen tetrachloroaureate(III) trihydrate [$HAuCl_4.3H_2O$] were purchased from Sigma-Aldrich and were used without further purification. MilliQ water was used as solvent for all solution preparation and sodium hydroxide [NaOH, Merck, 35%] was used to change the pH-value of the solution.

2.2 Preparations

AuNPs were prepared from mixed aqueous solution of TBP and gold salt at room temperature, by the method developed by Sakai et al.[17,18,25] As a first step, aqueous P123-solution of

Table 1 Parameters such as the average hydrodynamic diameter ($2R_{DLS}$), the SPR peak position (λ_{SPR}) and its saturation intensity ($I_{SPR,s}$, relative to the intensity at 460 nm), the critical growth time (τ) and the average size ($2R_{TEM}$) of the AuNPs prepared using P123-micellar solution of different pH-value as obtained from the DLS, optical absorption and TEM measurements.

pH-value	$2R_{DLS}$ (nm)	λ_{SPR} (nm)	$I_{SPR,r}$ (a.u.)	τ (min)	$2R_{TEM}$ (nm)
6.8	140	564	0.27	90	49
8.3	120	557	0.34	60	–
9.5	13 & 80	538	0.38	50	4 & 16
10.6	19	531	0.15	40	4 & 14
11.2	19	529	0.15	35	–
11.6	19	525	0.19	30	4 & 11

RSC Advances Accepted Manuscript

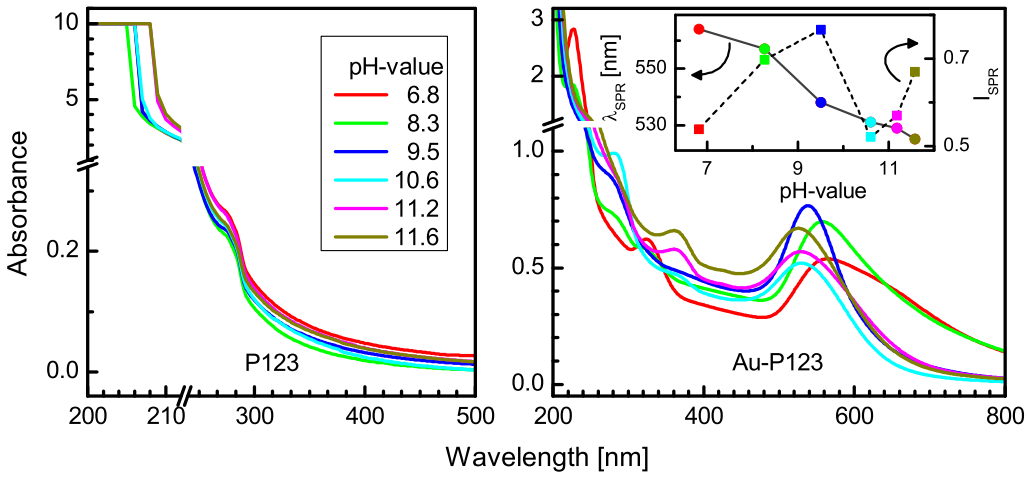

Fig. 2 UV-vis absorption spectra of the mixed binary (P123 + water) and ternary ($HAuCl_4$ + P123 + water) solutions of different pH values (data taken after 3 h of mixing). Inset: Variation of SPR peak position (λ_{SPR}) and its intensity (I_{SPR}) with pH-value.

concentration 5.75 mM (3.33% w/v) was prepared by magnetic stirring for 2 h and then aqueous $HAuCl_4$-solution of concentration 2 mM was prepared. It is to be noted that during synthesis of the AuNPs, the concentrations of the gold salt and P123 in the aqueous solutions were kept fixed, and only the pH-value of the P123 solution was varied within basic region. The pH-value of as-prepared aqueous P123-solution is 6.82. By adding different amount of NaOH-solution, the pH-value of P123-solution was varied (8.26, 9.50, 10.60, 11.18, 11.58) and measured using a pH meter. Finally, 45 ml of P123-solutions of different pH-values are mixed separately with 5 ml of $HAuCl_4$-solution and stirred for about 10 min. Then the mixed solutions were kept at ambient condition (∼25°C and ∼40%) for 3 h without any disturbances. The color of the solutions changed from colorless to pink-purple or purple within half an hour and remained the same thereafter in most cases. The pH-values reported in this paper were those of the aqueous P123-solutions before mixing with aqueous $HAuCl_4$-solution. The mixed solutions and P123-solutions of pH-value 6.82, 8.26, 9.50, 10.60, 11.18 and 11.58 are henceforth referred as pH ≈ 6.8, 8.3, 9.5, 10.6, 11.2 and 11.6, respectively.

2.3 Characterizations

DLS experiments were performed to probe the size variation of the micelles in the pure aqueous P123-solution with different pH values before and after addition of the aqueous $HAuCl_4$-solution. Also an idea about the size of the nanostructures formed by AuNPs and P123-micelles in the mixed solutions was obtained from DLS measurements. The measurements were carried out using Zetasizer (Nano-S, Malvern Instrument).[37] The light source was He-Ne laser operated at 633 nm with a maximum output power of 15 mW. Each measurement was repeated at least two times.

Time dependent UV-vis absorption spectra of the mixed solutions of $HAuCl_4$ + P123 + water were carried out with a UV-vis spectrophotometer (Lambda 750, Perkin Elmer).[36,37] For comparison UV-vis absorption spectra of the mixed solutions of P123 + water were also carried out. The instrument was operated in spectrum mode with a wavelength interval of 1 nm and the samples were held in quartz cuvettes of path length 1 cm. It makes use of a tungsten halogen lamp as the visible light source and a deuterium discharge lamp for the UV light source. Surface plasmon resonance (SPR) band determination of AuNPs[30,31] is one of the most familiar applications of this technique, which arises due to the resonance between the incident radiation and collective oscillation of conducting electrons of metal nanostructures.

The size and morphology of the nanostructures composed of AuNPs and P123-micelles were observed using TEM (Tecnai S-twin, FEI or JEM 2100 HR, JEOL), operating at an accelerating voltage of 200 kV. Prior to the TEM sample preparation, the solutions are centrifuged with water at 12,000 rpm for 20 min to remove the free P123-micelles from the solutions as much as possible. Samples were then prepared by placing a drop of gold colloids on a carbon-coated copper grid and allowed to dry in air. It should be noted that no staining agent, which is usually employed to observe clearly the micellar assemblies in order to build an appropriate contrast against the bright background, has been used in the present study. TEM micrographs were analyzed using ImageJ software.

3 Results and discussion

3.1 Dynamic light scattering

The particle size distribution plots, obtained from DLS measurements for all the mixed solutions after 3 h of mixing, are shown in Fig. 1. A single Gaussian-like peak with a narrow intensity size distribution and almost at same position is found for all the P123 micelles solutions suggesting not much variation in the size of the spherical shaped micelles with the pH-value of the aqueous solution. The average hydrodynamic diameter of the P123-micelles is found about 19 nm, which is consistent with the value observed before at normal pH.[24]

The intensity size distribution curve becomes highly pH-dependent when $HAuCl_4$ is added in the P123 micellar solution. Such distribution can be categorized in three pH regions.

RSC Advances Accepted Manuscript

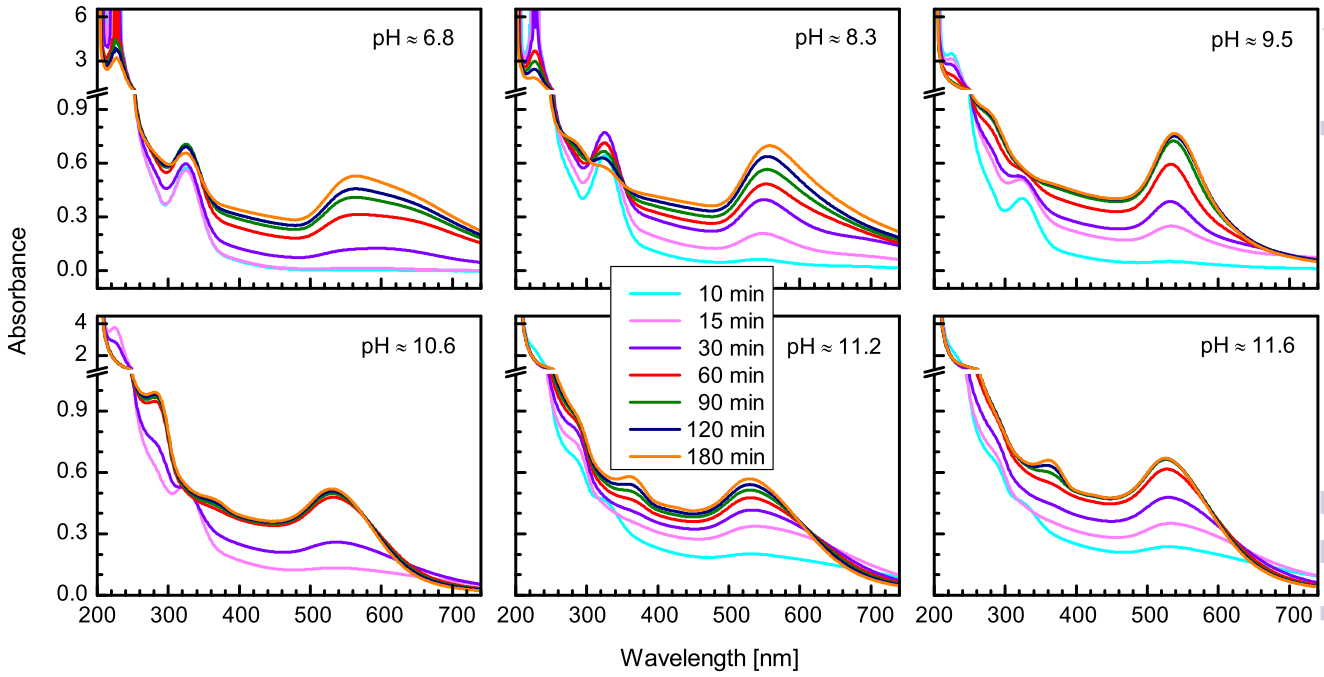

Fig. 3 Time-evolution UV-vis absorption spectra of the mixed ternary ($HAuCl_4$ + P123 + water) solutions of different pH values.

Region 1, for pH ≈ 6.8 and 8.3, where a single peak at large value (around 140 and 125 nm, respectively) is observed in the intensity-size distribution curves. Region 2, for pH value around 9.5, where dual peaks at around 13 and 80 nm are found in the intensity-size distribution curve and finally region 3, for pH values above 9.5, where a single peak at around 19 nm, similar to that of the free micelles, is found in the intensity-size distribution curves. This suggests that although there is not much influence of pH-value in the size and shape of free micelles in aqueous solution but strong influence in the size and shape of the nanostructures that are formed when $HAuCl_4$-solution is added into the micellar solution. The average hydrodynamic diameter ($2R_{DLS}$), that are observed for different pH-value, are tabulated in Table 1. At region 1, no peak corresponding to the size of the free micelles is observed. A single peak due to large size may originates from the self-aggregation of P123-micelles due to loading of AuNPs into the surface cavities or may be due to the formation of large AuNPs or agglomeration of small AuNPs. As the pH-value increases, the size of such nanostructures decreases. Also the intensity of the peak decreases, while its width increases, suggesting formation of smaller size nanostructures or aggregates with larger size-distribution when the pH-value increases. At region 2, a new peak at around 13 nm is formed along with the decreasing intensity and increasing size-distributed peak at around 80 nm. The appearance of the new peak is likely to be originated from free AuNPs. At region 3, the peak corresponding to the large size nanostructures or aggregates disappears completely. Inspite, a strong peak near 19 nm is only observed (the width of the peak is quite narrow but wider compared to the free micelles), which is probably related to the P123 capped AuNPs. Thus DLS measurements indicates that at high pH-values, large number of small-size (of about 19 nm) P123 coated AuNPs are formed. The information obtained from DLS measurements allows us to predict possible size of the nanostructures formed in different solutions, which is important. However, to know the detailed growth of AuNPs in solutions and their final shape and size distributions, analysis of time evolved UV-vis spectra and TEM images are very important, which have been presented next.

3.2 UV-vis spectroscopy

The UV-vis absorption spectra of the mixed solutions, collected after 3 h of mixing, are shown in Fig. 2. Two peaks are observed in the mixed binary (P123 + water) solutions of different pH-value, while several peaks are observed in the UV-vis spectra of the mixed ternary ($HAuCl_4$ + P123 + water) solutions of different pH-value. For the mixed binary solutions, saturation in the absorption intensity below 205-208 nm and presence of a low intensity peak or shoulder near 280 nm are observed. The intensities and positions of the strong and weak peaks near 205 and 280 nm, respectively, which arise due to P123,[26] are found to be same for all pH values. This suggests that though the environment of the micelles is modified, by adding different amount of NaOH in the solution, the intrinsic property of the P123 as well as the size of the micelles (as obtained from DLS study) do not alter much.

The peaks are mainly found near 205, 226, 284, 325 and 540 nm in the mixed ternary solutions (see Fig. 2). The intensities of which, however, varies with the pH-value. The peaks near 205 and 284 nm are similar to that of the bare micellar solutions and thus can be assigned to the P123. The intensity of the peak near 205 nm is very high (above saturation value) for all the solutions and thus can not be compared. The peak near 284 nm, on the other hand, become prominent or sharp with pH-value upto the value of pH ≈ 10.6, after which it al-

RSC Advances Accepted Manuscript

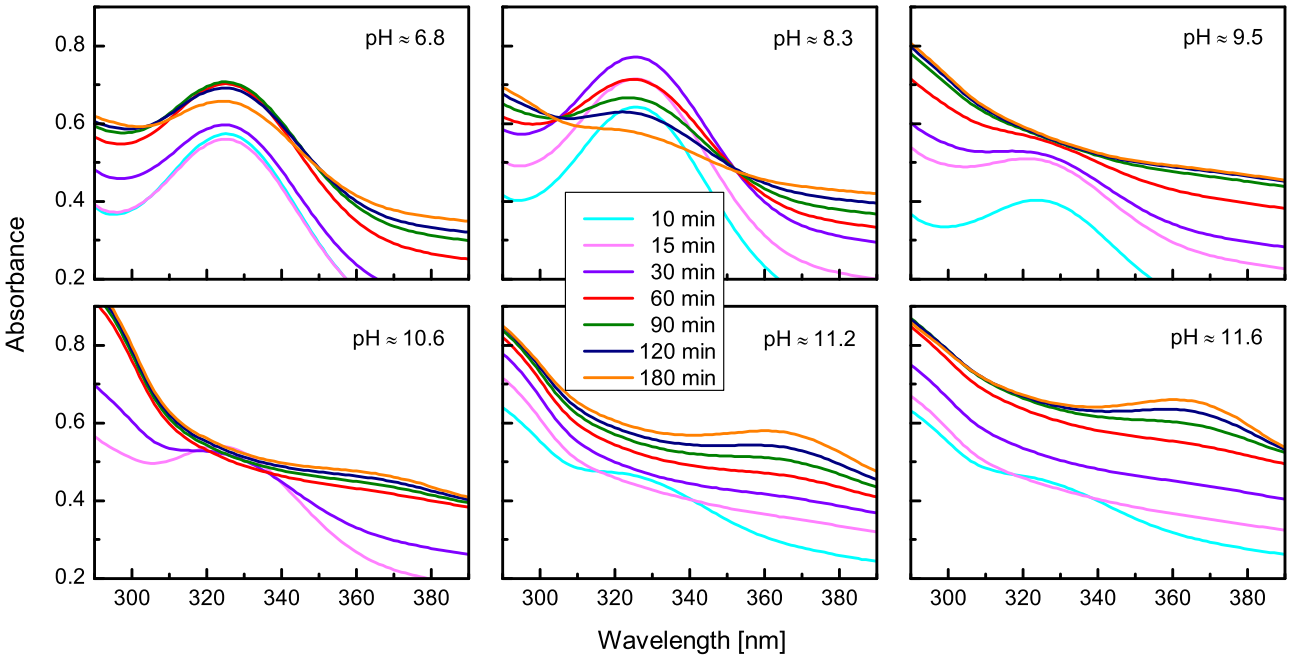

Fig. 4 Magnified view of the time-dependent UV-vis absorption spectra near 325 nm of the mixed ternary ($HAuCl_4$ + P123 + water) solutions of different pH values.

most disappear. The peaks around 226 and 325 nm are found for the ligand-to-metal charge transfer (LMCT) transitions in $AuCl_4^-$ ions and LMCT complexes. The latter is reported to form due to the interaction of $AuCl_4^-$ ion with the PEO chain of the surface cavity.[26,27,41,42] The signatures of peaks at 226 and 325 nm are prominent in the mixed solution of pH ≈ 6.8. Both the peaks become feeble and gradually disappear with the increase of pH. In spite, a new peak near 365 nm gradually appear, which is quite prominent for high pH. This band may arise due to the reduction in the energy gap between $2e_u(\pi) \rightarrow 2b_{1g}(\sigma^*)$ orbital caused by the complexation by the π-donor oxygen lone pairs of the PEO parts.[6,43] The peak near 540 nm corresponds to the well known surface plasmon resonance (SPR) of AuNPs. The position (λ_{SPR}), intensity (I_{SPR}), width and shape of which varies with the pH-value. The values of λ_{SPR} for different pH-value are tabulated in Table 1. The variation of λ_{SPR} and I_{SPR} with pH-value are shown in the inset of Fig. 2. The peak is blue shifted gradually (from 565 to 525 nm), with large change near pH ≈ 9.5, while the intensity of the peak first increases upto pH ≈ 9.5, then decreases suddenly and again increases with pH-value. Thus a transition in the SPR peak, similar to that of the size distribution (obtained from DLS study), is observed near pH ≈ 9.5. The blue shift of the SPR peak with pH-value is associated with the decrease in particle size. The width and shape of the SPR peak are found broad and asymmetrical for low pH-value. It is known that the longitudinal component of the SPR can arise at higher wavelength, due to anisotropic shape or chain-like aggregation of particles. However, for the anisotropic shaped particles, the intensity of longitudinal component must be high compared to the transverse component, which is not the case. Thus the observed broad asymmetric SPR peak can be due to the large size distribution or chain-like aggregation of particles. The shape of the peak becomes more symmetrical with the increase of pH-value, while the width of the peak decreases considerably upto the pH ≈ 9.5 and then increases slightly above it when the shape becomes almost symmetrical. Symmetrical shape of the peak is associated with narrow size distribution and less aggregation of particles, while the slight increase of the symmetrical peak width with pH-value is again associated with the decrease in the particle size.

The time-evolution UV-vis absorption spectra of the mixed ternary solutions, collected for different pH-value, are shown in Fig. 3 to understand the influence of pH-value of the aqueous solution of P123 micelles on the growth of AuNPs with time. Saturation in the intensity is observed below 205 nm for all spectra. Also, strong peak near 226 nm is observed for low pH-value solution at the initial stages, due to $AuCl_4^-$ ions, which decreases with time and pH-value. On the other hand, SPR peak near λ_{SPR}, due to the formation of AuNPs, evolved with time. Such peak is found very much broad and asymmetric for the low pH-value solution at the initial stages. With time and increasing pH-value, the peak becomes less broad and more symmetric. However, for the mixed solution of pH ≈ 6.8, the peak remains quite broad and asymmetric with time. This suggest that initially formed AuNPs have either large size distribution or chain-like aggregation or both. With time and increasing pH-value, however, spherical AuNPs with narrow size distribution and less aggregation, are formed. For the mixed solution of pH ≈ 6.8, no appreciable peak near 284 nm is observed throughout the time. The peak become visible with time as the pH-value of the solution increases and become prominent for pH ≈ 10.6. Above this pH-value, visible peak near 284 nm is observed initially, which remains almost unchanged with time. A prominent peak near 325 nm is observed for low pH-value

RSC Advances Accepted Manuscript

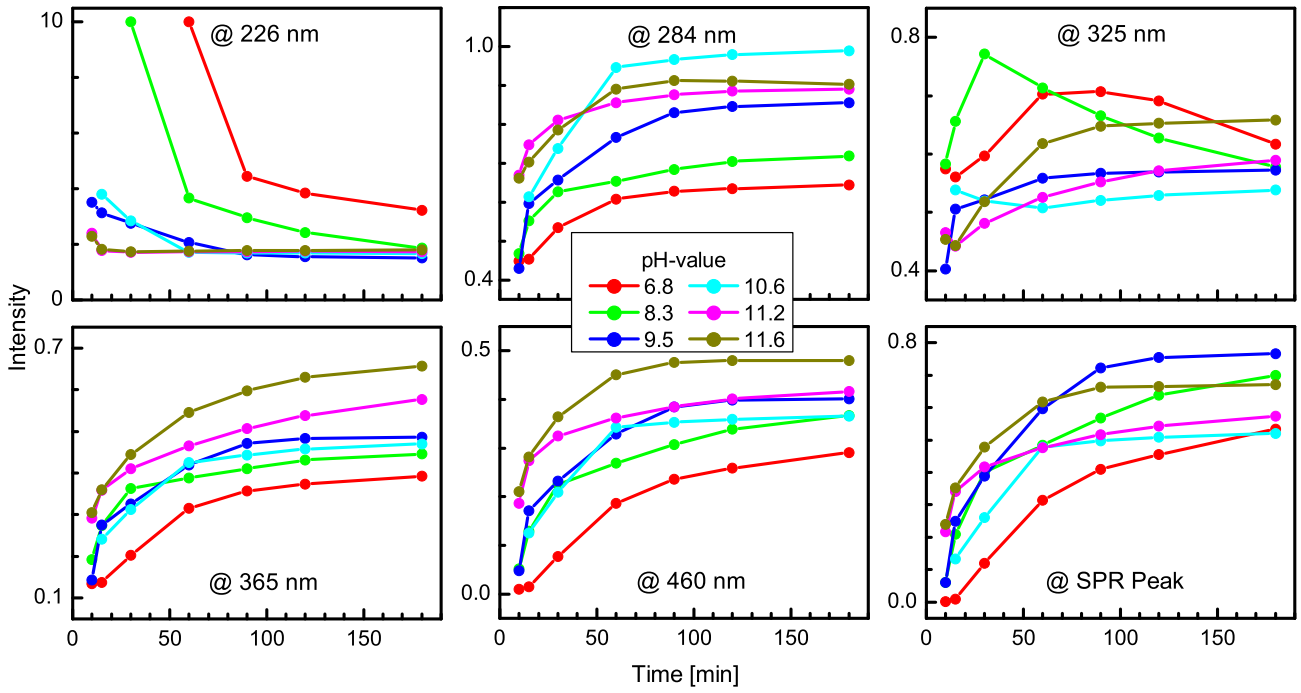

Fig. 5 Evolution of absorption intensity at 226, 325, 365, 284, 460 nm and SPR peak with time for the mixed ternary ($HAuCl_4$ + P123 + water) solutions of different pH values.

solution at the initial stages, due to LMCT complex, which become feeble and disappear with time and pH-value. In spite, a peak near 365 nm appear with time for high pH-value solutions. The signature of the peaks (near 325 nm and 365 nm) and their evolution with time for different pH-value solutions are clear from the magnified view of the UV-vis spectra near that region, as shown in Fig. 4. The increase in the intensity of the plateau-like region (near 380-460 nm) with time is also observed, which is mainly related to the increase in the total number of gold atoms in the solution, irrespective of their form.[44,45]

To get further understanding on the growth of AuNPs, evolution of absorption intensity at 226, 284, 325, 365, 460 nm and SPR peak with time for mixed ternary solutions of different pH-value are plotted in Fig. 5. The intensity at 226 nm and SPR peak are found to decrease and increase, respectively, with time, which were also obvious from the nature of the peaks and are well expected. However, the intensity at 284 nm and 365 nm are found to increase, which were not obvious from the nature of the peaks and are not expected. Similarly, the intensity at 325 nm, which is found first increasing then decreasing or gradually increasing with time, is not consistent with the nature of the peak or expectation. Such inconsistency is due to the evolution of the intensity near plateau-like region (shown by variation of intensity at 460 nm) with time, which sometime over shadowed the actual peak intensity. To get the actual peak variation, the contribution corresponding to the plateau-like region needs to be suppressed. The evolution of such relative intensity at 226, 284, 325, 365 nm and SPR peak (i.e. intensities relative to the intensity at 460 nm), with time for the mixed ternary solutions of different pH-value are shown in Fig. 6. It is clear from this figure that the intensity corresponding to both $AuCl_4^-$ ion (226 nm) and LMCT complex (325 nm) decreases, while that of the SPR of AuNPs ($I_{SPR,\,r}$) increases with time. The variation of $I_{SPR,\,r}(t)$ can be expressed quantitatively using standard exponential dependence,[46] namely $I_{SPR,\,r}(t) = I_{SPR,\,s}[1-\exp(-t/\tau)]$, where $I_{SPR,\,s}$ is the saturation intensity and τ is the critical growth time. Analyzed curves using above expression have been plotted in Fig. 5. The parameters $I_{SPR,\,s}$ and τ obtained from the analysis for different pH-value are tabulated in Table 1. For the solution of pH $\approx$ 6.8, the peak intensity at 226 nm decreases sharply upto about 90 min and then nearly saturates, while that at 325 nm decreases slowly. The intensity at SPR of AuNPs increases moderately with τ about 90 min. For the solution of pH $\approx$ 8.3, the sharp fall of the peak intensity at 226 nm takes place much earlier (before 60 min) and the decrease in the peak intensity at 325 nm is relatively fast, while the intensity at SPR of AuNPs increases relatively fast with τ about 60 min. For the solution of pH $\approx$ 9.5, the intensity of both the peaks (at 226 and 325 nm) is initially small, which decreases gradually then saturates. However, the intensity at SPR of AuNPs increases significantly with τ about 50 min. For the solution of pH $\approx$ 10.6, the decrease in the intensity (at 226 and 325 nm) is slightly fast, while the increase in the intensity (at SPR of AuNPs) is very low with τ about 40 min. For the solution of pH $\approx$ 11.2, the intensity of both the peaks (at 226 and 325 nm) is initially even small, which decreases very fast and saturates within 20 min, while the intensity at SPR of AuNPs increases fast with τ about 35 min. For the solution of pH $\approx$ 11.6, the behavior is similar to that of pH $\approx$ 11.2. However, the increase in the intensity (at SPR of AuNPs) is even more and fast with τ about 30 min. The intensity of the peak at 28[illegible] nm remains almost unchanged with time for all the solutions,

RSC Advances Accepted Manuscript

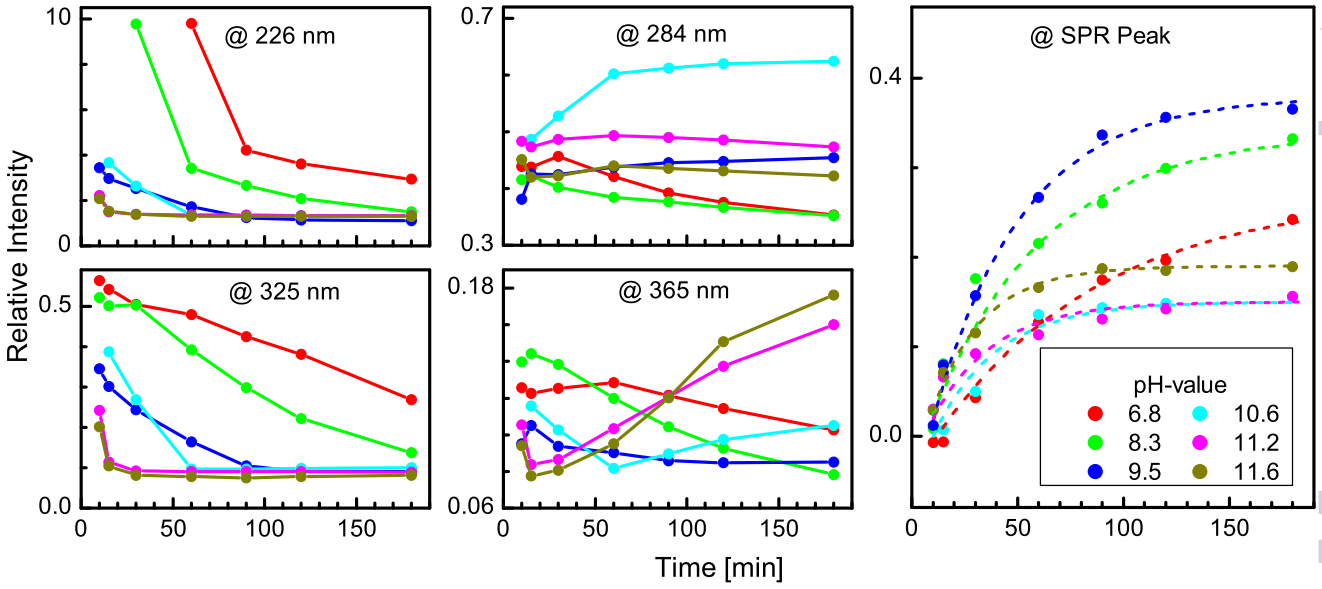

Fig. 6 Evolution of absorption intensity at 226, 284, 325, 365 nm and SPR peak (relative to the intensity at 460 nm) with time for the mixed ternary ($HAuCl_4$ + P123 + water) solutions of different pH values. Solid line through the data is to guide the eye, while dashed lines through the data is the analyzed curve.

with exception for pH ≈ 10.6, where it first increases with time and then saturates. The intensity of the peak at 365 nm remains nearly same or decreases slightly with time for most of the solutions, with exception for the high pH-value solutions, where peak increases after some time. For the solution of pH ≈ 10.6, small increase takes place after 60 min but the final value is less that of the initial one, while for pH ≈ 11.2 and 11.6, increase takes place after 20 min and the final value is relatively high. At the initial stages, the intensity of the peaks at 226 and 325 nm decreases considerably with pH-value, while that of the SPR of AuNPs do not increases to that extent, rather the intensity at 460 nm (i.e. for the plateau-like region) increases appreciably. At the final stages, the intensity of the SPR of AuNPs first increases gradually with pH-value upto 9.5, then decreases suddenly and again increases little bit with pH-value. The large decrease in the intensity for the high pH-value solutions is mainly counterbalance by the increase in the intensity at the plateau-like region and 365 nm, while for the solution of pH ≈ 10.6, the increase in the intensity is only at 284 nm.

3.3 Transmission electron microscopy

Typical TEM images, in different resolution, for the samples prepared from the mixed ternary ($HAuCl_4$ + P123 + water) solutions of different pH-value are shown in Fig. 7. Formation of isolated AuNPs (dark spots), free P123-micelles (lighter spots) and small AuNPs loaded large P123-micelles or micellar assemblies (dark spots in lighter contrast) are evident in the TEM images. However, the size of the isolated AuNPs is found to vary significantly with the pH-value. Particle size distribution histogram for the isolated AuNPs and their average size ($2R_{TEM}$), as obtained from the log-normal distribution for the different pH-value mixed solutions are shown in the insets of Fig. 7 and also tabulated in Table 1. Formation of AuNPs or gold nanocrystals is further confirmed from the selected area diffraction pattern as shown in Fig. 7d. For the sample prepared from the solution of pH ≈ 6.8, the average size of the AuNPs is found (see Fig. 7a-c) well-faceted, relatively large (about 49 nm), less uniform and slightly interconnected. In the same sample presence of free P123-micelles (of size about 19 nm) is also obvious along with the isolated AuNPs (see Fig. 7b). For the samples prepared from the solutions of pH ≈ 9.5, 10.6 and 11.6 (s Fig. 7e-g, i-k, m and n), the average size of the isolated AuNPs are found 16, 14 and 11 nm, respectively, which are quite small. Also the presence of free P123-micelles is observed (see Fig. 7e) in these samples. Additionally, very small AuNPs (less than 4 nm) incorporated in large P123 micelles are also observed in these samples, which are not found in the sample of pH ≈ 6.8.

It can be noted that the observed TEM results support well the findings of both DLS and UV-vis results. As predicted from the DLS and UV-vis results, TEM results confirmed the formation of isolated AuNPs, the average size of which decreases with the increasing pH-value, with transition around pH ≈ 9.5. Below and above this pH-value, the size of the isolated AuNPs are relatively big and small, respectively. However, the size es.. mated from TEM ($2R_{TEM}$) is less than that estimated from DLS ($2R_{DLS}$) and can be understood as follows. The size that we observed in the DLS measurements is the hydrodynamic diameter. So, it can overestimate the size due to polymer coating and/or chain-like aggregation. Large objects of $2R_{DLS} > 100$ nm, i the low pH-values, is probably due to such chain-like conne.. tivity, as TEM images show the formation of AuNPs of $2R_{TEM} \approx$ 49 nm with some connectivity and also the optical absorpti.. spectra show asymmetric shape of SPR peak. While the overestimation of the small object of $2R_{DLS} \approx 19$ nm, in the large p.. values, is probably due to the polymer coating. Additionally, t.. very small AuNPs, those are found incorporated in large P123-

RSC Advances Accepted Manuscript

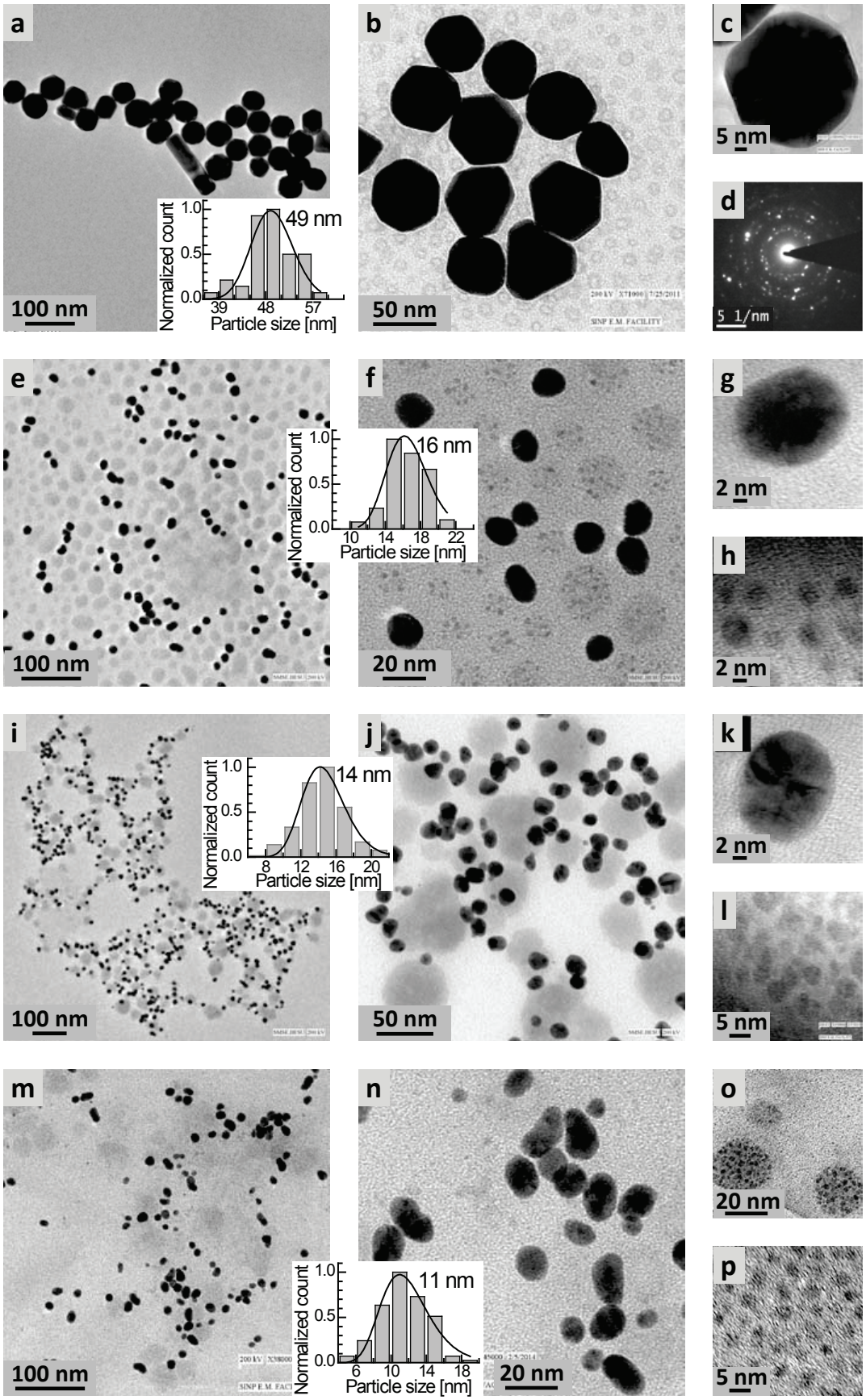

Fig. 7 Typical TEM images in different resolutions and selected area diffraction pattern showing formation of isolated AuNPs and also small AuNP loaded large P123 micelles in the mixed ternary ($HAuCl_4$ + P123 + water) solutions of different pH value. (a)−(d) for pH ≈ 6.8, (e)−(h) for pH ≈ 9.5, (i)−(l) for pH ≈ 10.6 and (m)−(p) for pH ≈ 11.6. Insets: Corresponding size histogram of isolated AuNPs and their average size, as obtained from log-normal distribution.

RSC Advances Accepted Manuscript

micelles in the high pH-values (from the TEM images) suggest that at high pH-values not all Au-ions after reduction form isolated AuNPs. Rather some remain very small and trapped in the micelles and some even stay in the near atomic states. Accordingly, in the VU-vis spectra, the intensity of the SPR peak is found relatively less and the intensity near 460 nm or 365 nm is found relatively high.

3.4 Formation and growth of AuNPs in TBP solution

The results clearly show that the pH-value of the P123 micellar solution has significant influence on the reduction rate of gold ions, growth and stabilization of the AuNPs and on the final self-assembly of the nanoparticle-micelles nanocomposite. This is schematically illustrates in Fig. 8. In order to understand this in details, let us first discuss the proposed formation mechanism of AuNPs from mixed aqueous solution of gold salt and TBP-micelles in a single step synthesis process.

Generally, the strong tetrachloroauric(III) acid totally dissolved in aqueous solution generating complex $AuCl_4^-$ ions of square planar geometry and produce two absorption bands at 226 and 315 nm in UV-vis absorption spectra corresponding to the $p_\sigma \rightarrow 5d_{x^2-y^2}$ (i.e. $\sigma \rightarrow \sigma*$) and $p_\pi \rightarrow 5d_{x^2-y^2}$ (i.e. $\pi \rightarrow \sigma*$) LMCT transitions, respectively.[47] First one is quite strong compared to the second one. It was reported earlier that, in aqueous solution this $AuCl_4^-$ ion undergoes a pH dependent stepwise hydrolysis, in which replacement of chloride by hydroxide ligand takes place and formation of $[AuCl_x\ (OH)_{4-x}]^-$ complex ion occurs.[27,41,42,48] Accordingly, both the absorption bands were found to shift toward the lower wavelength value with the increase of pH-value.[27,41,42,48] However, in this study, no such shift is found. In fact, only the relatively strong lower wavelength band is observed, which remains fixed at 226 nm, indicating formation of only $AuCl_4^-$ ions and no $[AuCl_x\ (OH)_{4-x}]^-$ complex ions even in high-pH values. Thus it is clear that, unlike the high pH-value of the aqueous solution of gold salt, the high pH-value of the aqueous P123-solution do not convert the $AuCl_4^-$ ions to $[AuCl_x\ (OH)_{4-x}]^-$ complex ions.

On the other hand, the TBP-monomers, above the critical micelle concentration (cmc), aggregate in the aqueous solution to form well-defined micelles. The corona of the TBP-micelle is composed of hydrophilic PEO units arranged in the form of surface cavities (pseudo-crown ether structure) which can bind the $AuCl_4^-$ ions and acts as sites for the site-specific redox reaction because of the presence of ether oxygens.[5,12] The redox reaction, involving the reduction of $AuCl_4^-$ ions and oxidation of the oxyethylene and oxypropylene segments of TBP micelles initiates the synthesis of the nucleating centers of AuNPs in the PEO-PPO-PEO surface cavities. The nucleating centers then undergo growth process to produce AuNPs.[21,25] There are several processes for the growth of low dimensional structures in general.[3,7,25,49–52] Formation of AuNPs in solution, in presence of sodium borohydride, is proposed through a rapid conversion of the ionic gold precursor into metallic gold nuclei, followed by particle growth via coalescence of smaller entities.[51] Growth of AuNPs in presence of TBP-micelles may occurs between the nucleating centers occupying the neighboring surface cavities

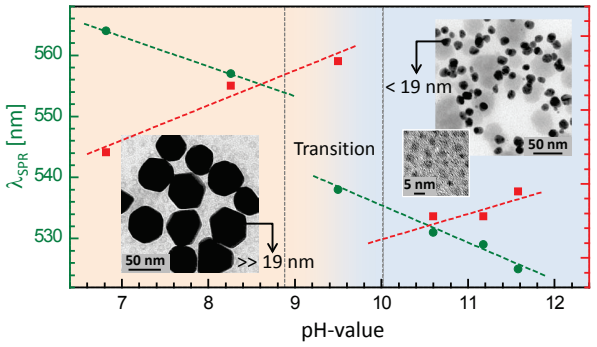

Fig. 8 Schematic illustration of the pH-dependent size and structural transition in P123-micelles induced AuNPs, showing transition around pH ≈ 9.5 from slowly grown, well-faceted, large (>> 19 nm), less uniform and near connected to fast grown, near symmetrical, small (< 19 nm), more uniform and well separated AuNPs, and also few trapped very small (< 4 nm) AuNPs.

or through autocatalytic thermodynamically controlled reduction (ATCR) or both depending upon micelle environment, size and shape of micellar assemblies.[17–19] It can be noted that the formation of nanoparticles within solution can occur through LaMer nucleation, Finke-Watzky two step mechanism, Ostwald ripening, digestive ripening, coalescence and orientated attachment, and intraparticle growth.[52] However, the prediction of the nanoparticle formation mechanism is still questionable, as a small change in the reaction condition can lead to a completely different mechanism.[52]

Here the micellar solutions of high pH-values (pH ≥ 6.8, i.e. toward basic region) are prepared first and then the aqueous gold solution is mixed in it and not the aqueous gold solutions of high pH-values directly. In such conditions high pH-values do not convert $AuCl_4^-$ ions into $[AuCl_x\ (OH)_{4-x}]^-$ complex ions and the appearance of the band at 325 nm is not due to the shift of the 315 nm band, rather it is due to the $AuCl_4^-$ ions bind with the PEO chains in the surface cavities. The pH-value of the micellar solution strongly influence the reduction of $AuCl_4^-$ ions and thus the nucleation and subsequent growth process to produce stable AuNPs with narrow size distribution and well-defined morphology. When the pH-value of the solution is low (here about 6.8) then the conversion of $AuCl_4^-$ ions to Au atoms [i.e. reduction of Au(III) to Au(0)] after binding with the PEO chains of the surface cavities [i.e. Au(I)] is relatively slow and incomplete. Such slow process seems to create less number of Au(0) nucleation centers, which then grow slowly but enough through the ATCR of gold ions on the surface of available nucleating centers present in the surface cavity of the micelle and subsequently through the diffusion and coalescence to create relatively large and well-faceted AuNPs of different shape, which can not be supported by the soft small micelles. Initially formed AuNPs have chain-like aggregations of different chain length, which with time grow to form more symmetrical and relatively large stable AuNPs of size much greater than that (about 19 nm) of the free micelles. As the pH-value of the solution increases, the reaction rate and the conversion becomes fast and nearly complete. Accordingly, the number of

RSC Advances Accepted Manuscript

nucleation centers increases, while the growth of the centers is restricted by the limited amount of available gold ions for the further ATCR in one hand and the interplay between the metal-polymer hdrophobic and polymer-water hydrophilic interactions on the other hand (to optimize the entropy and the free energy of the solution). Above the transition pH-value ($\approx$ 9.5) this restriction seems to be prominent. As a result, the controlled growth of the centers takes place through ATCR and diffusion followed by early capping through near individual micelles to form isolated symmetric small AuNPs of size less than that (about 19 nm) of the free micelles, with narrow size distribution. The size of such AuNPs further decreases slowly with the increase of the pH-value due to the increase of the reaction rate and hence the number of nucleation centers. Although, from our recent study it is very difficult to pin point in favour of a particular growth mechanism, nonetheless, from different experimental evidences and also considering the shape of the size distribution, it can be inferred that the growth is through ATCR, diffusion and coalescence. The diffusion is dominant in the initial phases and is prominent for the high pH values (where the growth is fast and the capping takes place early), while the coalescence is dominant in the latter stages and is prominent for the low pH values (where the growth is slow and takes place for relatively long time).

It can be noted that at high pH-value although the conversion of $AuCl_4^-$ ions to Au atoms is fast and nearly complete (as observed from the optical absorption intensity at 226 and 325 nm), but not all the Au atoms (though majority) grow to form isolated AuNPs (as observed from SPR peak intensity). Rather the faster reduction rate of gold ions and simultaneous complete conversion of LMCT complex to Au(0), produce large number of nucleating centers within the surface cavity of the micelle and promote intermicelle fusion to produce some hybrid micelles of larger size. The surface cavity of the micelle acts as soft template to form very small AuNPs (of size less than 4 nm) by entrapping some of the nucleating centers in its micellar phase (as observed from the optical absorption intensity at 365 and 460 nm and also from TEM images of very small AuNPs trapped miceller assemblies). It is necessary to mention that above the transition pH-value, isolated AuNPs of small size (less than 19 nm) with narrow size distribution are formed, but at the same time there remains a significant amount of gold after reduction in very small sizes (formed in the early stages) and trapped inside the micellar assemblies and/or in the near atomic states, which are of real concern and needs further study to improve the yield of the isolated small AuNPs by reducing the amount of such trapped and near atomic states gold.

4 Conclusions

The role of pH-value of the aqueous solution of P123-micelles, in the growth and formation of the AuNPs, in a single-step synthesis process, is evaluated using time-evolution UV-vis spectroscopy, DLS and TEM techniques. The basic medium of the P123-micelles converts the $AuCl_4^-$ ions to Au atoms [i.e. reduction of Au(III) to Au(0)] after binding them with the PEO chains of the surface cavities [i.e. Au(I)]. Initially converted Au atoms then acts as nucleation centers, which subsequently grow through ATCR of gold ions on the surface of available nucleating centers, diffusion and/or coalescence to form stable AuNPs. However, the conversion or reduction rate is found to depend strongly on the pH-value, which essentially controls the growth of the AuNPs. For the pH-value less than 9.5, the reduction rate is slow and the number of nucleation centers is less, which through subsequent ATCR, diffusion and coalescence, formed well-faceted near symmetrical large AuNPs of size much greater than that of the free P123-micles. For the pH-value above 9.5, the reduction rate of the gold ions is fast and the number of nucleation centers is large. Controlled growth of the centers takes place through ATCR (of the limited amount of available gold ions) and diffusion followed by early capping through near individual micelles to form isolated symmetrical small AuNPs of size $<$ 19 nm, with narrow size distribution, by optimizing the entropy and the free energy of the solution having large numbers of nucleation centers due to fast reduction, further growth through ATCR and the metal-polymer and polymer-water interactions. Additionally, a large number of nucleating centers within the surface cavity of the micelles also promote the intermicelles fusion to produce some hybrid micelles of larger size, where very small size AuNPs are trapped. Such trapped AuNPs and/or the observed near atomic states Au which cannot grow further, limited the yield of the intended isolated small AuNPs.

Acknowledgements

The authors thank Prof. P. M. G. Nambissan and Ms. Soma Roy for their help in UV-vis measurements, Prof. M. Mukherjee for extending the DLS facility and Mr. Pulak Ray, Prof. N. R. Bandyopadhyay and CRNN, University of Calcutta for TEM measurements.

References

1 S. Chen, C. Guo, G. H. Hu, J. Wang, J. H. Ma, X. F. Liang, L. Zheng and H. Z. Liu, *Langmuir*, 2006, **22**, 9704.

2 X. Ji, X. Song, Y. Bai, W. Yang and X. Peng, *J. Am. Chem. Soc.*, 2007, **129**, 13939.

3 B. K. Pong, H. I. Elim, J. X. Chong, W. Ji, B. L. Trout and J. Y. Lee, *J. Phys. Chem. C*, 2007, **111**, 6281.

4 K. Rahme, F. Gauffre, J. D. Marty, B. Payre and C. Mingotuad, *J. Phys. Chem. C*, 2007, **111**, 7273.

5 P. Alexandridis, *Chem. Eng. Technol.*, 2011, **34**, 15.

6 T. S. Sabir, D. Yan, J. R. Milligan, A. W. Aruni, K. E. Nick, R. H. Ramon, J. A. Hughes, Q. Chen, R. Kurti and C. C. Perry, *J. Phys. Chem. C*, 2012, **116**, 4431.

7 H. Koerner, R. I. MacCuspie, K. Park and R. A. Vaia, *Chem. Mater.*, 2012, **24**, 981.

8 E. C. Dreaden, A. M. Alkilany, X. Huang, C. J. Murphy and M. A. El-Sayed, *Chem. Soc. Rev.*, 2012, **41**, 2740.

9 K. Saha, S. S. Agasti, C. Kim, X. Li and V. M. Rotello, *Chem. Rev.*, 2012, **112**, 2739.

10 I. Ojea-Jiménez, X. López, J. Arbiol and V. Puntes, *ACS Nano*, 2012, **6**, 2253.

RSC Advances Accepted Manuscript

11 P. Zhao, N. Li and D. Astruc, *Coord. Chem. Rev.*, 2013, **257**, 638.

12 M. S. Bakshi, *Adv. Colloid Interface Sci.*, 2014, **213**, 1.

13 M. Brust, M. Walker, D. Bethell, D. J. Schiffrin and R. Whyman, *J. Chem. Soc., Chem. Commun.*, 1994, 801.

14 K. Torigoe and K. Esumi, *Langmuir*, 1992, **8**, 59.

15 R. A. Caruso, M. Ashokkumar and F. Grieser, *Langmuir*, 2002, **18**, 7831.

16 T. Ishii, H. Otsuka, K. Kataoka and Y. Nagasaki, *Langmuir*, 2004, **20**, 561–564.

17 T. Sakai and P. Alexandridis, *Langmuir*, 2004, **20**, 8426.

18 T. Sakai and P. Alexandridis, *Langmuir*, 2005, **21**, 8019.

19 P. Khullar, A. Mahal, V. Singh, T. S. Banipal, G. Kaur and M. S. Bakshi, *Langmuir*, 2010, **26**, 11363.

20 D. Ray, V. K. Aswal and D. Srivastava, *J. Nanosci. Nanotechnol.*, 2010, **10**, 6356.

21 P. Khullar, V. Singh, A. Mahal, H. Kaur, V. Singh, T. S. Banipal, G. Kaur and M. S. Bakshi, *J. Phys. Chem. C*, 2011, **115**, 10442.

22 S. Dey, A. Adhikari, U. Mandal, S. Ghosh and K. Bhattacharyya, *J. Phys. Chem. B*, 2008, **112**, 5020.

23 D. Ray, V. K. Aswal and J. Kohlbrecher, *Langmuir*, 2011, **27**, 4048.

24 S. Mandal, C. Ghatak, V. G. Rao, S. Ghosh and N. Sarkar, *J. Phys. Chem. C*, 2012, **116**, 5585.

25 T. Sakai and P. Alexandridis, *J. Phys. Chem. B*, 2005, **109**, 7766.

26 Q. Shou, C. Guo, L. Yang, L. Jia, C. Liu and H. Liu, *J. Colloid Interface Sci.*, 2011, **363**, 481.

27 S. Wang, K. Qian, X. Z. Bi and W. Huang, *J. Phys. Chem. C*, 2009, **113**, 6505.

28 W. P. Halperin, *Rev. Mod. Phys.*, 1986, **58**, 533.

29 P. Mulvaney, *Langmuir*, 1996, **12**, 788.

30 S. Link and M. A. El-Sayed, *J. Phys. Chem. B*, 1999, **103**, 8410.

31 S. Hazra, A. Gibaud and C. Sella, *Appl. Phys. Lett.*, 2004, **85**, 395.

32 S. Hazra, *Appl. Surf. Sci.*, 2006, **253**, 2154.

33 S. Hazra, A. Gibaud and C. Sella, *J. Appl. Phys.*, 2007, **101**, 113532.

34 W. Haiss, N. T. K. Thanh, J. Aveyard and D. G. Fernig, *Anal. Chem.*, 2007, **79**, 4215.

35 V. Amendola and M. Meneghetti, *J. Phys. Chem. C*, 2009, **113**, 4277.

36 I. Roy and S. Hazra, *Soft Matter*, 2015, **11**, 3724.

37 I. Roy and S. Hazra, *RSC Adv.*, 2015, **5**, 665.

38 W. Brown, *Dynamic Light Scattering: The Method and Some Applications*, Clarendon Press, Oxford, 1993.

39 B. J. Berne and R. Pecora, *Dynamic Light Scattering*, Dover Publications, New York, 2000.

40 A. Gibaud, S. Hazra, C. Sella, P. Laffez, A. Désert, A. Naudon and G. V. Tendeloo, *Phys. Rev. B*, 2001, **63**, 193407.

41 D. V. Goia and E. Matijevic, *Coll. Surf. A*, 1999, **146**, 139.

42 I. Ojea-Jiménez, F. M. Romero, N. G. Bsatús and V. Puntes, *J. Phys. Chem. C*, 2010, **114**, 1800.

43 H. Isci and W. R. Mason, *Inorg. Chem.*, 1983, **22**, 2266.

44 C. F. Bohren and D. R. Huffman, *Absorption and Scattering of Light by Small Particles*, Wiley-Interscience, New York, 1983.

45 Y.-Y. Fong, J. R. Gascooke, B. R. Visser, G. F. Metha and M. A. Buntine, *J. Phys. Chem. C*, 2010, **114**, 15931.

46 P. Chatterjee and S. Hazra, *J. Phys. Chem. C*, 2014, **118**, 11350.

47 A. K. Gangopadhayay and A. Chakravorty, *J. Chem. Phys.*, 1961, **35**, 2206.

48 S. Ivanova, C. Petit and V. Pitchon, *Appl. Catal. A-Gen.*, 2004, **267**, 191.

49 J. K. Basu, S. Hazra and M. K. Sanyal, *Phys. Rev. Lett.*, 199?, **82**, 4675.

50 J. K. Bal and S. Hazra, *Phys. Rev. B*, 2009, **79**, 155412.

51 J. Polte, R. Erler, A. F. Thünemann, S. Sokolov, T. T. Ahner, K. Rademann, F. Emmerling and R. Kraehnert, *ACS Nano*, 2010, **4**, 1076.

52 N. T. K. Thanh, N. Maclean and S. Mahiddine, *Chem. Rev.*, 2014, **114**, 7610.

RSC Advances Accepted Manuscript